Inorganic Chemistry

ARTICLE

pubs.acs.org/IC

Revisiting the Zintl−Klemm Concept: Alkali Metal Trielides

Fei Wang and Gordon J. Miller*

Department of Chemistry, Iowa State University, Ames, Iowa 50011, United States

Supporting Information

ABSTRACT: To enhance understanding of the Zintl−Klemm concept, which is useful for characterizing chemical bonding in semimetallic and semiconducting valence compounds, and to more effectively rationalize the structures of Zintl phases, we present a partitioning scheme of the total energy calculated on numerous possible structures of the alkali metal trielides, LiAl, LiTl, NaTl, and KTl, using first-principles quantum mechanical calculations. This assessment of the total energy considers the relative effects of covalent, ionic, and metallic interactions, all of which are important to understand the complete structural behavior of Zintl phases. In particular, valence electron transfer and anisotropic covalent interactions, explicitly employed by the Zintl−Klemm concept, are often in competition with isotropic, volume-dependent metallic and ionic interaction terms. Furthermore, factors including relativistic effects, electronegativity differences, and atomic size ratios between the alkali metal and triel atoms can affect the competition by enhancing or weakening one of the three energetic contributors and thus cause structural variations. This partitioning of the total energy, coupled with analysis of the electronic density of states curves, correctly predicts and rationalizes the structures of LiAl, LiTl, NaTl, and KTl, as well as identifies a pressure-induced phase transition in KTl from its structure, based on $[Tl_6]^{6-}$ distorted octahedra, to the double diamond NaTl-type.

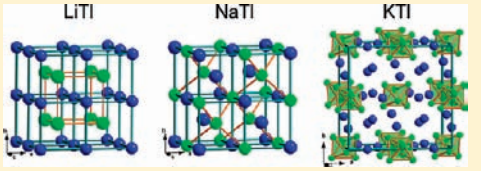

INTRODUCTION

One significant goal of solid-state science is to design and prepare materials with desired properties. Because properties are the expression of crystal and electronic structures, with the latter deduced from the former through quantum mechanics, it is essential to possess a sound understanding of the structures of solids, as well as the forces that govern the aggregation of atoms into structures, which can change in response to variations in chemical composition and external conditions. Solids have been traditionally categorized into three model classes, ionic, metallic, and covalent, each of which employs different structural rationalizations. However, there are no clear dividing lines because the variations among the three classes are gradual rather than abrupt. They can even be described using the same theoretical model. Burdett[1] has argued that metals, just like covalent species, can be described with a tight-binding scheme; their energy bands are also formed through orbital overlap. So, there is no essential difference between "covalent bonds" and "metallic bonds", except that in metals the driving force for distortions of the electron density is too small to cause electron localization and opening of band gaps in the electronic density of states. Such continuities among metallic, ionic, and covalent interactions mean that there are solids that can exhibit metallicity, ionicity, and covalency simultaneously and cannot be approximated into any one of these three model classes, for instance, Zintl phases. For such intermediate solids, the complete structural rationalization becomes challenging.

Zintl phases are compounds composed of electropositive metals (e.g., alkali, alkaline earth, or rare earth metals) and electronegative metals or semimetals around the "Zintl line", that is, the line dividing groups 13 and 14.[2−9] They keep intriguing solid-state chemists for many reasons, one of which is that they are promising in many applications especially as thermoelectric materials.[10−15] The structures of Zintl phases can be understood using the Zintl−Klemm concept. As an example, consider the most frequently quoted Zintl phase, NaTl,[16] which adopts a double diamond structure with Na and Tl forming interpenetrating diamond substructures. The Zintl−Klemm rationalization of NaTl is that Na donates its 3s electron to Tl, resulting in a formal Tl^- anion with 4 valence electrons. This "anion" behaves as a pseudotetrel atom, each of which forms 4 covalent bonds and adopts the diamond structure. Each Na^+ "cation" acts as a charge balancer and space filler.

Although simplistic, the Zintl−Klemm concept decently rationalizes the structures of Zintl phases. The validity of this concept was confirmed by first-principles calculations on K−Sb,[17] K−Sn,[18] and K−Te systems.[19] Its success stems from its consideration of charge transfer and covalent interactions in intermetallic compounds, implying that Zintl phases, although composed of metallic or semimetallic elements, also involve ionic and covalent interactions. Thus, Zintl phases are a compound class bridging metallic, ionic, and covalent substances. Also, indeed, Zintl phases exhibit features resembling nonmetallic solids, for example, narrow homogeneity ranges or "precise" compositions and poor conductivity or semiconductivity.[14]

The Zintl−Klemm concept, however, also has limitations. For instance, LiTl,[20] isoelectronic with NaTl, adopts a CsCl-type

Received: March 29, 2011
Published: July 20, 2011

dx.doi.org/10.1021/ic200643f | Inorg. Chem. 2011, 50, 7625–7636

structure, which defies the Zintl−Klemm concept, whereas LiAl,[21] LiGa,[22] and LiIn[23] all adopt the NaTl-type structure at ambient conditions. Moreover, the Zintl−Klemm concept does not predict a unique structure for a given chemical composition. For example, besides the cubic diamond structure, the hexagonal diamond or lonsdaleite structure also satisfies the Zintl−Klemm formalism for Tl^-. Also, KTl adopts a structure thoroughly different from LiTl or NaTl and contains Tl_6 distorted octahedra[24] with local point symmetry C_{2h}. Every Tl atom can still be perceived as four-bonded, and, indeed, Si atoms form similar octahedral clusters in the gas phase.[25] So, the Zintl−Klemm rule in KTl is formally obeyed, but it cannot explain the cause of the difference between KTl and NaTl, which become isostructural under pressures higher than 2 kbar.[26] Such structural effects of external pressure on Zintl phases have not yet been discussed. These limitations stem from the oversimplification of the Zintl−Klemm concept, which considers charge transfer but does not take into complete account the subsequent interactions between "cations" and "anions", as in ionic crystals. That is, the Zintl−Klemm rationalization focuses on the covalent interactions between "anions", while the structural effect of "cations" is overlooked. However, the difference between LiTl and NaTl indicates that this influence should not be overlooked. Furthermore, Zintl phases are composed of metals or semimetals, so they are expected to retain metallic character. For instance, NaTl has an electrical conductivity of $1.23 \times 10^{-4}\ \Omega^{-1}\ cm^{-1}$ at 20 °C, and it decreases with increasing temperature.[27] Thus, such compounds unlikely build up highly charged cations and anions. Therefore, to rationalize the structures and properties of Zintl phases, we must comprehensively evaluate ionicity, metallicity, and covalency.

In this contribution of a reassessment of the Zintl−Klemm formalism, we focus on the alkali metal trielides, LiAl, LiTl, NaTl, and KTl, using first-principles density functional theory. We present an approach that is more sophisticated than simply counting valence electrons and covalent bonds, but evaluates the effects of metallicity and covalency by partitioning the calculated total energy into an electrostatic term and an electronic term. In addition to an analysis of the observed structural behavior, we consider phase transitions under pressure and viable alternative structures, which may be acceptable under the Zintl−Klemm formalism. Finally, we compare a spectrum of structures for these four alkali metal trielides, structures that frequently occur among typical metallic, ionic, and covalent crystals. With these efforts in this Article and a forthcoming paper,[28] we intend to provide better insights of the structures of Zintl phases by analyzing the full Zintl−Klemm concept using quantum mechanical calculations.

COMPUTATIONAL DETAILS

1. VASP Calculations. The Vienna ab initio simulation package (VASP)[29−31] was employed to calculate the energies, band structures, and valence electron density maps of model structures of LiAl, LiTl, NaTl, and KTl. All calculations utilized projector augmented-wave (PAW) pseudopotentials[32] and the Perdew−Burke−Ernzerhof generalized gradient approximation (PBE-GGA).[33] Energies and total charge densities were integrated in reciprocal space with a $7 \times 7 \times 7$ Monkhors−-Pack *k*-points mesh.[34] The energy cutoffs for calculating energies and optimizing structures are 240.3 eV for LiAl, 140.0 eV for LiTl, 102.0 eV for NaTl, and 116.7 eV for KTl. This affords a convergence in total energy to less than 1 meV per atom. To calculate band structures and valence electron maps for LiAl, LiTl, and NaTl in the NaTl-type structure, the energy cutoffs are set to higher values: 300.4 eV for LiAl, 175.0 eV for LiTl, and 127.5 eV for NaTl. All band structures and valence electron density maps were plotted with wxDragon.[35] Structural optimizations were exerted upon the noncubic model structures (see section 3: Model Structures) to determine their aspect ratios and atomic positions for each of the four compositions. During these optimizations, the volumes of the unit cells were fixed and the conjugate gradient algorithm[36] was applied. Energy versus volume, $E(V)$, curves were plotted and fitted to the Murnaghan equation of state,[37] from which we could determine the equilibrium volumes V_{eq}, that is, the volume at the minimum of an $E(V)$ curve. Electronic structure calculations were then completed upon model structures at V_{eq} values.

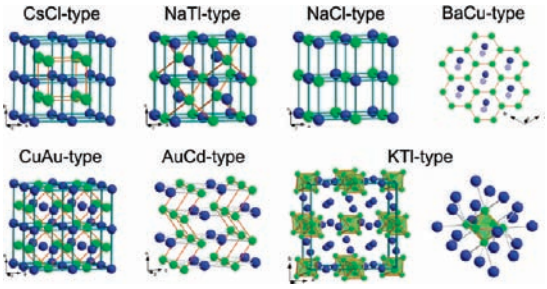

Figure 1. The seven structure types investigated. Blue, Li/Na/K; green, Al/Tl.

2. LMTO Calculations. We used the Stuttgart Tight-Binding, Linear-Muffin-Tin Orbital program with Atomic Sphere Approximation (TB-LMTO-ASA)[38] to calculate the electronic density of states (DOS) and crystal orbital Hamiltonian population (COHP)[39] curves. We also analyzed covalency effects by calculating integrated COHP (ICOHP) values, which scale with the energy lowering due to pairwise orbital overlap. This lowering is with respect to the energies of electrons in noninteracting valence atomic orbitals, and not to the homogeneous electron gas. However, because the valence atomic orbitals are not an orthogonal set, ICOHP values depend on the position of the origin of the energy scale of these calculations and are unreliable for calculating covalent energy terms between different chemical systems.[39−42] Nevertheless, our approach is to compare ICOHP values for identical compositions in structures with equal volumes per fu and Wigner−Seitz radii for the atoms. We postulate that such relative ICOHP values evaluated in this way can be used to analyze the stabilization caused by covalent interactions. However, any analysis of relative ICOHP values is supplemented by consideration of the total electronic energy and its partitioning.

For all TB-LMTO-ASA calculations, the exchange and correlation energy was treated with the von Barth−Hedin local density approximation.[43] All relativistic effects except spin−orbit coupling were taken into account using a scalar relativistic approximation.[44] The basis sets included the valence s and p orbitals of all elements: Li 2s and 2p; Na and Al 3s and 3p; K 4s and 4p; and Tl 6s and 6p. The Wigner−Seitz radii of atomic spheres were adjusted by an automatic procedure,[45] and empty spheres were generated where they were necessary so that the unit cells were filled by Wigner−Seitz spheres with overlaps ranging from 7.55% to 10.22%. The first Brillouin zone was sampled with an $8 \times 8 \times 8$ *k*-points mesh.

3. Model Structures. Seven model structures, NaTl-, KTl-, BaCu-, CsCl-, NaCl-, CuAu- (fcc), and AuCd-type (hcp), illustrated in Figure 1, were studied for each of the four compositions, LiAl, LiTl, NaTl, and KTl. For each composition, the seven model structures were built with equal volumes per formula unit (V_{fu}), which were taken from the experimental values.[16,20,21,24] Structural details of these models are listed

dx.doi.org/10.1021/ic200643f |*Inorg. Chem.* 2011, 50, 7625–7636

Table 1. Structural Details of Model Structures Used for Calculations

structure	atom	Wyck.	x	y	z	structure	atom	Wyck.	x	y	z
NaTl-type, $Fd\bar{3}m$, $a = (8\ V_{fu})^{1/3}$	Li/Na/K	8a	0	0	0	CsCl-type, $Pm\bar{3}m$,	Li/Na/K	1a	0	0	0
	Al/Tl	8b	1/2	1/2	1/2	$a = (V_{fu})^{1/3}$	Al/Tl	1b	1/2	1/2	1/2
KTl-type,[a] $Cmce$, $a = (24V_{fu}(a/b)(a/c))^{1/3}$,	Li/Na/K1	8e	1/4	y	1/4	NaCl-type, $Fm\bar{3}m$,	Li/Na/K	4a	0	0	0
$b = (b/a)a$, $c = (c/a)a$	Li/Na/K2	8d	x	0	0	$a = (4V_{fu})^{1/3}$	Al/Tl	4b	1/2	1/2	1/2
	Li/Na/K3	8f	0	y	z						
	Al/Tl1	16g	x	y	z	AuCd-type, $Pmma$,	Li/Na/K	2f	1/4	1/2	5/6
	Al/Tl2	8f	0	y	z	$b = (2V_{fu}/(8)^{1/2})^{1/3}$,	Al/Tl	2e	1/4	0	1/3
						$a = (8/3)^{1/2}b$, $c = (3)^{1/2}b$					
BaCu-type,[a] $P6_3/mmc$,	Li/Na/K	4f	1/3	2/3	z	CuAu-type, $P4/mmm$,	Li/Na/K1	1a	0	0	0
$a = (((8V_{fu})/(3)^{1/2})(a/c))^{1/3}$,	Al/Tl1	2b	0	0	1/4	$a = c = (2V_{fu})^{1/3}$	Li/Na/K2	1c	1/2	1/2	0
$c = (c/a)a$	Al/Tl2	2d	1/3	2/3	3/4		Al/Tl	2e	0	1/2	1/2

[a] The aspect ratios, b/a and c/a, are determined by structural optimizations with VASP.

in Table 1. Among the seven structure types, the NaTl-, the CsCl-, and the NaCl-structures are cubic, and all atoms are located at symmetrically special sites, so the only variable for these structures is V_{fu}. The CuAu-type is tetragonal, but we made $a = c$ so that it is ideally fcc. For the AuCd-type (hcp) structure, besides V_{fu}, the aspect ratio (c/a) is also a free variable. We set $c/a = (8/3)^{1/2}$ so that it has an ideal hcp geometry. There are more degrees of freedom in the KTl- and the BaCu-type structures, which contain, respectively, Tl_6 distorted octahedral clusters and planar 6^3 nets of Cu. After setting V_{fu}, the aspect ratios (c/a and b/a) and atomic coordinates (x, y, and z) remain variable. To determine these structural parameters, we executed structural optimization with VASP. The details of optimized KTl- and BaCu-type structures can be found in the section Results and Discussion and in the Supporting Information.

RESULTS AND DISCUSSION

1. Partitioning the Total Energy in VASP. VASP conveniently calculates the metallic electrostatic energy (E_{ES}),[46,47] which is defined as the electrostatic energy in a system composed of positive cores and a homogeneous valence electron gas (HEG). It includes the repulsion between cores and the attraction between the cores and HEG:

$$E_{ES} = V_{core-core} + V_{core-HEG} \quad (1)$$

This term reflects the effect of the "metallic interaction". By subtracting E_{ES} from the total energy (E_{TOT}), which includes core−core repulsion, core−valence electron (VE) attraction, interactions between valence electrons (Coulomb, exchange, and correlation), and the kinetic energy of valence electrons:

$$E_{TOT} = V_{core-core} + V_{core-VE} + V_{VE-VE} + T_{VE} \quad (2)$$

we obtain the electronic energy term ($E_{electronic}$):

$$\begin{aligned} E_{electronic} &= E_{TOT} - E_{ES} \\ &= V_{core-VE} - V_{core-HEG} + V_{VE-VE} + T_{VE} \end{aligned} \quad (3)$$

which can be rewritten as:

$$\begin{aligned} E_{electronic} = {} & (V_{core-VE} - V_{core-HEG}) \\ & + (V_{VE-VE} - V_{HEG-HEG}) \\ & + (T_{VE} - T_{HEG}) + V_{HEG-HEG} + T_{HEG} \end{aligned} \quad (4)$$

The first three terms in parentheses are the contributions to the electronic energy caused by the difference between real valence electrons and the homogeneous electron gas, or by valence electron inhomogeneity, that is, localization, which includes covalent bonding, charge transfer (ionicity), formation of lone pairs, etc. The last two terms are the energy of homogeneous electron gas alone, terms that are independent from the positions of atoms and, as such, have no relationship with structure types. The kinetic energy of homogeneous electron gas, T_{HEG}, is a functional of valence electron density, n:[48]

$$T_{HEG} = 3^{5/3}\pi^{4/3}\frac{\hbar^2}{10m}Vn^{5/3} \quad (5)$$

$V_{HEG-HEG}$ depends on n and the volume per fu, and it can be calculated as:[49]

$$V_{HEG-HEG} = \frac{n^2}{2}\iint\frac{d\mathbf{r}\ d\mathbf{r}'}{|\mathbf{r}-\mathbf{r}'|} \quad (6)$$

Table 2. Comparison of Energy Terms between hcp and Diamond Structures for Na and Si

compositions	V (Å^3/atom)	energy terms	hcp	diamond
Na		E_{ES} (eV/fu)	−6.6808	−6.2629
	37.80	$E_{electronic}$ (eV/fu)	0.2161	0.2193
		E_{TOT} (eV/fu)	**−6.4647**	−6.0436
Si		E_{ES} (eV/fu)	−120.8270	−112.5655
	20.03	$E_{electronic}$ (eV/fu)	13.1953	4.0853
		E_{TOT} (eV/fu)	−107.6317	**−108.4802**

If we compare $E_{electronic}$ of several iso-compositional structures at equal volumes per fu (so n also equal), the last two terms will make no difference because they are independent of structure types but only depend on n and volume. The difference among $E_{electronic}$ values will, thus, mainly come from the first three terms, the differences in valence electron localization among the various structures. This outcome can be confirmed by our results of VASP calculations on Na and Si (Table 2).

The valence electrons for Na, which is close to an ideal metal, closely resemble a homogeneous electron gas (VE ≈ HEG). The energy caused by valence electron localization is, therefore, close to zero, and the electronic energy term is:

$$E_{electronic} \approx V_{HEG-HEG} + T_{HEG} \quad (7)$$

We compared the real Na (hcp) and a hypothetical diamond-type Na at the same volume per fu (37.80 Å^3/fu[50]). As discussed above, $V_{HEG-HEG}$ and T_{HEG} do not differentiate between structure types. So, $E_{electronic}$ of hcp and diamond-type Na are

dx.doi.org/10.1021/ic200643f |Inorg. Chem. 2011, 50, 7625–7636

expected to be very close to each other. The difference in E_{TOT} will be mainly from E_{ES}. This is exactly what we see in Table 2, which shows that the two structures have almost equal $E_{electronic}$ but that E_{ES} is lower in hcp, so that hcp has the lower E_{TOT} and is the preferred structure.

By contrast, for two iso-compositional phases, which exhibit strong covalent interactions, valence electron densities deviate significantly from the homogeneous electron gas, so the first three terms in eq 4 are not zero and $E_{electronic}$ depends on the positions of atom cores, that is, structure types. The comparison between real Si (diamond-type) and a hypothetical hcp Si (Table 2) at equal volumes per atom (20.03 Å^3/atom[51]) shows that, although E_{ES} is still lower for hcp, $E_{electronic}$ values are significantly different and counteract E_{ES}, even overruling it, and rendering a lower E_{TOT} for the diamond structure.

Therefore, by partitioning E_{TOT} into E_{ES} and $E_{electronic}$, and comparing these values at equal volumes per fu, we can segregate the effects of metallic interactions out by examining E_{ES} to see which structure is favored if valence electrons are highly delocalized. We can also evaluate the effects of valence electron localization by examining $E_{electronic}$. This includes both covalency and ionicity, which cannot be further separated into energy terms with only VASP. Yet we can analyze the ionicity effects by calculating the ionic Madelung energy with the Ewald technique[52] assuming a +1 charge on each alkali metal atom and a −1 charge on each triel atom and evaluate the covalency effects using LMTO calculations.

2. LiAl, LiTl, and NaTl: CsCl versus NaTl Structure Types. The NaTl- and the CsCl-type structures both occur for alkali metal trielides. These two structure types are closely related: atoms occupy the same positions and only differ in the way they are distributed among these positions in the two structures (or, in short, different "coloring schemes"[53]). The competition between these two structures has been studied by many researchers.[54−58] Some of these works based their arguments upon "size effects".[55−57] The rationalization is that the NaTl-type structure is obtained when the two following conditions are satisfied: (1) the larger atom is compressible, and (2) the radius ratio between the larger atom and the smaller atom is close to 1. These will ensure "contact" between the smaller atoms and stabilize the structure.

Other reports, just as this work, partitioned energy in different ways and rationalized that the competition between the two structures is a result of the competition between different energy terms.[54,58] Inglesfield's argument[54] is based on the interplay between the two energy terms $U_{metallic}$ and U_{sc}. $U_{metallic}$ is the band energy assuming a spherical Fermi surface, that is, assuming the compound is a simple metal whose electrons behave like a free electron gas. U_{sc}, named as "semiconductor term", is the energy caused by the formation of band gaps. $U_{metallic}$ prefers the CsCl-type structure, and U_{sc} favors the NaTl-type structure. Inglesfield also pointed out by calculating the bonding charge that electrons are expected to concentrate between triel atoms, so Zintl's covalent bonding picture is justifiable. However, he did not demonstrate how covalent bonding should affect those energy terms. In fact, U_{sc} is an evaluation of bonding because, from a chemist's view, the formation of a band gap in the DOS is often the result of covalent bonding; bonding states are lowered and antibonding states are raised in energy, generating a gap in the DOS.

Using the TB-LMTO-ASA method, Christensen[58] partitioned the total energy into an ionic Madelung term and a band energy term. The Madelung term is lower in the CsCl-type structure. So ionicity favors the CsCl-type structure. Counteracting the Madelung term, the band energy is always lower in the NaTl-type structure. Christensen claimed that this indicates that covalent bonding prefers the NaTl-type structure because the band energy "contains all the effects of bonding and hybridization". The effect of any metallic term was not discussed here. Actually, it is improper to assign the band energy term solely to covalency. The effect of metallic interactions may also be reflected here. For example, for hcp Na, the total energy calculated with LMTO is −323.81 Ry per atom, which is entirely from the band energy, because the ionic Madelung energy term is 0. Here, the band energy depicts a metallic picture because we do not expect significant covalent bonding in Na. In Zintl phases, where metallicity and covalency coexist, the band energy quantifies both effects. To complete Christensen's methodology, metallic electrostatic energy should be evaluated. Our results in the next section show that metallicity favors the CsCl-type structure. So the CsCl-type structure is also a better choice for metallic interactions. Therefore, that the band energy is lower in the NaTl-type structure is not because of metallicity. Christensen's conclusion is right after all: covalency favors the NaTl-type structure.

Table 3. Difference in Energy Terms, $\Delta E = E$(NaTl-type) − E(CsCl-type), between the CsCl- and NaTl-type Structures in LiAl, LiTl, and NaTl Calculated at Three Fixed Volumes, Which Are the Experimental Volumes of LiAl, LiTl, and NaTl

composition	energy terms	31.84 Å^3/fu	40.64 Å^3/fu	51.61 Å^3/fu
LiAl	ΔE_{TOT} (eV/fu)	−0.1553	−0.1747	−0.1363
	ΔE_{ES} (eV/fu)	1.3064	1.2054	1.1131
	$\Delta E_{electronic}$ (eV/fu)	−1.4617	−1.3801	−1.2494
LiTl	ΔE_{TOT} (eV/fu)	0.3952	0.1985	0.0716
	ΔE_{ES} (eV/fu)	1.3075	1.2054	1.1131
	$\Delta E_{electronic}$ (eV/fu)	−0.9123	−1.0069	−1.0415
NaTl	ΔE_{TOT} (eV/fu)	−0.0158	−0.0454	−0.0446
	ΔE_{ES} (eV/fu)	1.3076	1.2054	1.1131
	$\Delta E_{electronic}$ (eV/fu)	−1.3234	−1.2508	−1.1577

While all of these efforts systematically studied the two structure types, it remains unexplained why LiTl is the only one that adopts the CsCl-type structure. Substitution of Li for Na or Tl for other trields both result in the NaTl-type structure. Apparently, covalency is overruled by metallicity and/or ionicity in LiTl but not in the other alkali metal trielides. To investigate this, we compared LiTl with LiAl and NaTl. The comparisons were made between the two structure types at equal volumes per fu. The experimental volumes per fu of LiAl (31.84 Å^3/fu),[21] LiTl (40.64 Å^3/fu),[20] and NaTl (51.61 Å^3/fu)[16] were taken. At each volume, the NaTl- and the CsCl-type model structures were built, calculated, and compared for each of the three compositions: LiAl, LiTl, and NaTl.

The comparison of energy terms calculated with VASP is tabulated in Table 3. The total energy (ΔE_{TOT}) values predict the right structures; at all three volumes, the NaTl-type structure has lower energy in LiAl and NaTl (ΔE_{TOT} negative) but higher in LiTl (ΔE_{TOT} positive). Therefore, the competition between the NaTl- and the CsCl-type structures in alkali metal trielides cannot be attributed solely to a size effect as in some of the previous reports[55−57] mentioned above. Even if we equalize the size effect, they still favor different structures.

The metallic electrostatic energy values are always lower for the CsCl-type structure (ΔE_{ES} always positive) for all compositions

and volumes, indicating that metallic interaction favors the CsCl-type structure. The electronic terms are always lower for the NaTl-type structure ($\Delta E_{electronic}$ always negative). Although $\Delta E_{electronic}$ contains factors from both ionic and covalent interactions, its favoritism toward the NaTl-type structure must originate from covalency because, as mentioned above, ionicity favors the CsCl-type structure. So, covalent bonding stabilizes the NaTl-type structure, and it is competing with metallic and ionic interactions. Also, covalency wins in LiAl and NaTl ($\Delta E_{electronic}$ overcomes ΔE_{ES}) but loses in LiTl (ΔE_{ES} overcomes $\Delta E_{electronic}$).

We then examined the covalent interactions between the triel atoms by calculating the ICOHP values with LMTO (Table 4) and also by plotting the valence electron density maps (Figure 2) with VASP, which show close correspondence with each other. From the charge density maps, above all, we can see that Zintl–Klemm's covalent bonding picture is justifiable, especially for LiAl at 31.84 Å^3/fu; valence electrons are concentrated between Al atoms within cylindrical regions along Al–Al axial directions, a picture of chemical bonds. This is in sharp contrast with the CsCl-type structures (Supporting Information), in which valence electrons are enriched within slightly distorted spherical regions centered on triel atoms. Therefore, the NaTl-type structure has stronger Al/Tl–Al/Tl orbital interactions than the CsCl-type structure. Corresponding to this, the ICOHP values in Table 4 suggest that the Al/Tl–Al/Tl interaction in the NaTl-type structure lowers energy more significantly (i.e., more negative ICOHP) than in the CsCl-type structure. Note, however, that the ΔICOHP values cannot be numerically compared to $\Delta E_{electronic}$ (see section 2 of Computational Details).

We can also see that size has an effect. At larger volumes (longer triel–triel distances), valence electrons are distributed more around the triel atoms and less between them, that is, a weaker covalent interaction. Correspondingly, ICOHP also gets less negative (Table 4) at larger volume. However, size is not the only affecting factor. Tl and Al atoms do not behave the same even at the same volume: Tl–Tl interactions are weaker than Al–Al, which can be seen from the valence electron density map and suggested by ICOHP values. Pawlowska reported similar results calculated with the LMTO method.[59]

The ΔICOHP (= ICOHP(NaTl-type) − ICOHP(CsCl-type)) values in Table 4 also show the same pattern as $\Delta E_{electronic}$ in Table 3: at each volume, LiTl and NaTl have less negative ΔICOHP values than LiAl, demonstrating that, relative to the CsCl-type structure, the NaTl-type structure provides less stabilization in the thallides than in the aluminide through covalent interactions. The cause of such difference between the thallides and the aluminide can be found by comparing the band structures of NaTl-type LiAl, LiTl, and NaTl (Figure 3). Figure 3 shows that these band structures are similar except around the special *k*-points Γ (0, 0, 0) and *L* (π/a, π/a, π/a). The bands at these two *k*-points are examined in detail by projecting them onto the spherical harmonics (valence orbitals) of each atom and plotting their electron density maps (Supporting Information). Irreducible representation symbols taken from the Bilbao Crystallographic Sever[60] were assigned to these bands according to their eigenvectors.

Table 4. Triel–Triel ICOHP Values Calculated for LiAl, LiTl, and NaTl in Toth the CsCl- and the NaTl-type Structures with LMTO Method[a]

composition	ICOHP (eV/fu)	31.84 Å^3/fu	40.64 Å^3/fu	51.61 Å^3/fu
LiAl	$ICOHP_{Al-Al}$(CsCl-type)	−1.56	−1.24	−0.96
	$ICOHP_{Al-Al}$(NaTl-type)	−3.35	−2.76	−2.17
	$\Delta ICOHP_{Al-Al}$	−1.79	−1.52	−1.21
	$ICOHP_{s-s}$(NaTl-type)	−0.06	0.08	0.13
LiTl	$ICOHP_{Tl-Tl}$(CsCl-type)	−1.10	−0.88	−0.69
	$ICOHP_{Tl-Tl}$(NaTl-type)	−2.36	−2.00	−1.59
	$\Delta ICOHP_{Tl-Tl}$	−1.26	−1.11	−0.90
	$ICOHP_{s-s}$(NaTl-type)	0.33	0.32	0.25
NaTl	$ICOHP_{Tl-Tl}$(CsCl-type)	−1.19	−0.95	−0.74
	$ICOHP_{Tl-Tl}$(NaTl-type)	−2.75	−2.25	−1.74
	$\Delta ICOHP_{Tl-Tl}$	−1.56	−1.30	−1.00
	$ICOHP_{s-s}$(NaTl-type)	0.31	0.31	0.23

[a] ΔICOHP = ICOHP(NaTl-type) − ICOHP(CsCl-type). $ICOHP_{s-s}$ is the ICOHP of Al 3s–3s interactions and Tl 6s–6s interactions.

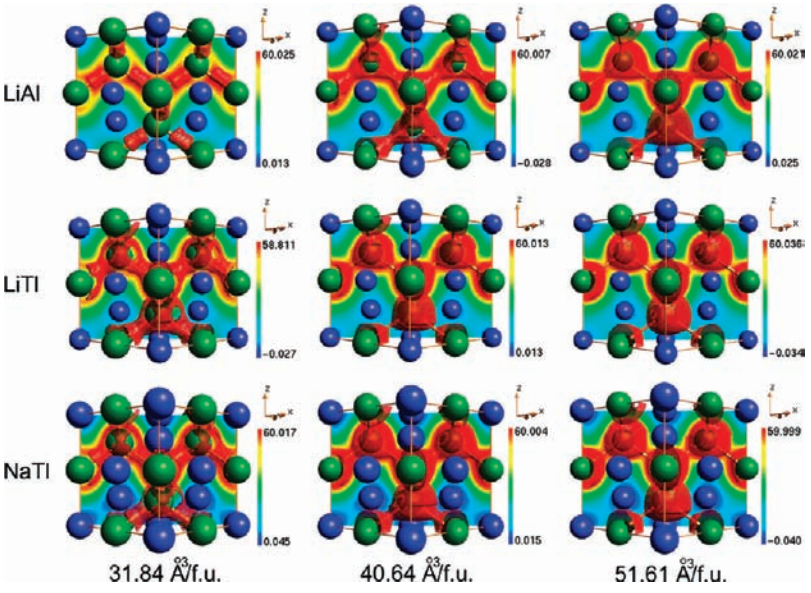

Figure 2. Valence electron density maps of NaTl-type LiAl, LiTl, and NaTl calculated with VASP.

dx.doi.org/10.1021/ic200643f |*Inorg. Chem.* 2011, 50, 7625–7636

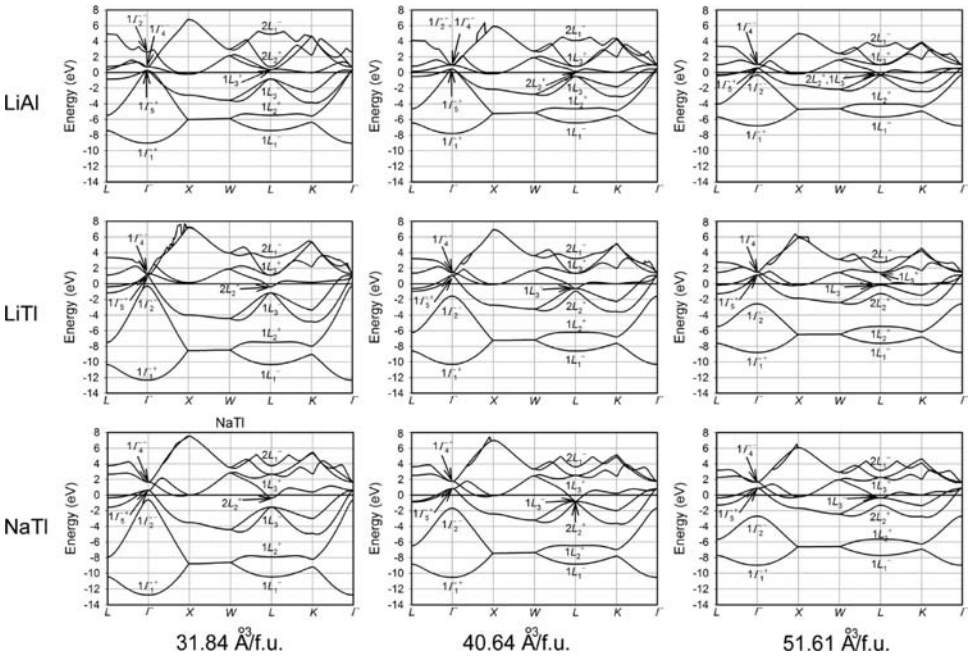

Figure 3. Band structures of NaTl-type LiAl, LiTl, and NaTl calculated with VASP.

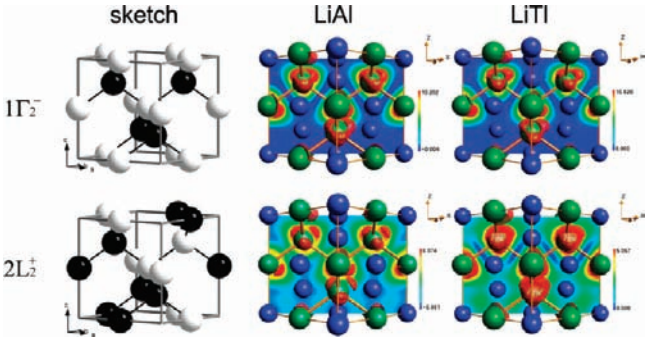

Figure 4. The crystal orbital sketches and valence electron density maps of $1\Gamma_2^-$ and $2L_2^+$ bands in LiAl (at 31.84 Å^3/fu) and NaTl-type LiTl (at 40.64 Å^3/fu). Only Tl/Al s orbitals are shown because Tl/Al p orbitals and Li orbitals have much smaller contributions (Supporting Information). Black and white colors specify the phase relationships. Blue, Li; green, Al/Tl.

Special attention was drawn to $1\Gamma_2^-$ and $2L_2^+$ bands, which are always below the Fermi level (E_F) in thallides, but above E_F in LiAl except at 51.61 Å^3/fu. The eigenvectors of these two bands are tabulated in the Supporting Information. Both $1\Gamma_2^-$ and $2L_2^+$ are mainly composed of the Al/Tl s orbitals. Crystal orbital sketches can be drawn for these two bands according to their eigenvectors, with Al/Tl s orbitals represented as spheres and the phase relationships specified with black and white color (Figure 4). $1\Gamma_2^-$ is clearly antibonding with every s orbital surrounded by four other s orbitals with opposite phase. $2L_2^+$ is partially antibonding; every s orbital is surrounded by one in-phase and three opposite-phase s orbitals. The valence electron density maps (also in Figure 4, only LiAl and LiTl are shown, NaTl is similar to LiTl) are consistent with the sketch; electron density depletion can be found between neighboring Al/Tl atoms in both LiAl and NaTl-type LiTl for these two bands. Therefore, s−s antibonding states are empty in aluminides

Table 5. IDOS Values of Each Atom in NaTl-type LiTl and NaTl Calculated with LMTO Method

composition	IDOS (E_F) (/fu)	31.84 Å^3/fu	40.64 Å^3/fu	51.61 Å^3/fu
LiTl	Li	1.30	1.16	1.06
	Tl	2.70	2.84	2.94
NaTl	Na	1.05	1.00	0.94
	Tl	2.95	3.00	3.06

(except at large volume) but populated in thallides, rendering weaker interactions between Tl atoms and less stabilization through covalency in thallides. This should be attributed to the fact that for Tl, its 6s orbital is more low-lying in energy with respect to 6p orbitals due to its poor shielding effect of 5d and 4f electrons and its strong relativistic effects.[61] The ICOHP values (Table 4) agree with this conclusion. The $ICOHP_{s-s}$ values of Tl−Tl interactions are always higher than those of Al−Al interactions. It is worth mentioning here that, opposite to the scalar relativistic effects that weaken Tl−Tl bonding and destabilize the NaTl-type structure, the relativistic spin−orbit coupling can provide electronic stabilization, as reported in our previous review.[62]

Additionally, the two thallides do not exhibit equal covalent interactions. Both $\Delta E_{electronic}$ (Table 3) and ΔICOHP (Table 4) are less negative in LiTl than in NaTl, showing that LiTl has less stabilization through Tl−Tl covalent interactions than NaTl. This can be rationalized by comparing the charge transfer from the alkali metal atom to Tl. Table 5 lists the IDOS(E_F) values of each atom in NaTl-type LiTl and NaTl. These numbers do not show exactly the number of valence electrons on each atom, because when IDOS is calculated, the "overlap population" is always evenly divided between atoms,[63] and this leads to overestimation for electropositive atoms and underestimation for electronegative atoms. Yet, they are still informative. By comparing the IDOS

dx.doi.org/10.1021/ic200643f |Inorg. Chem. 2011, 50, 7625–7636

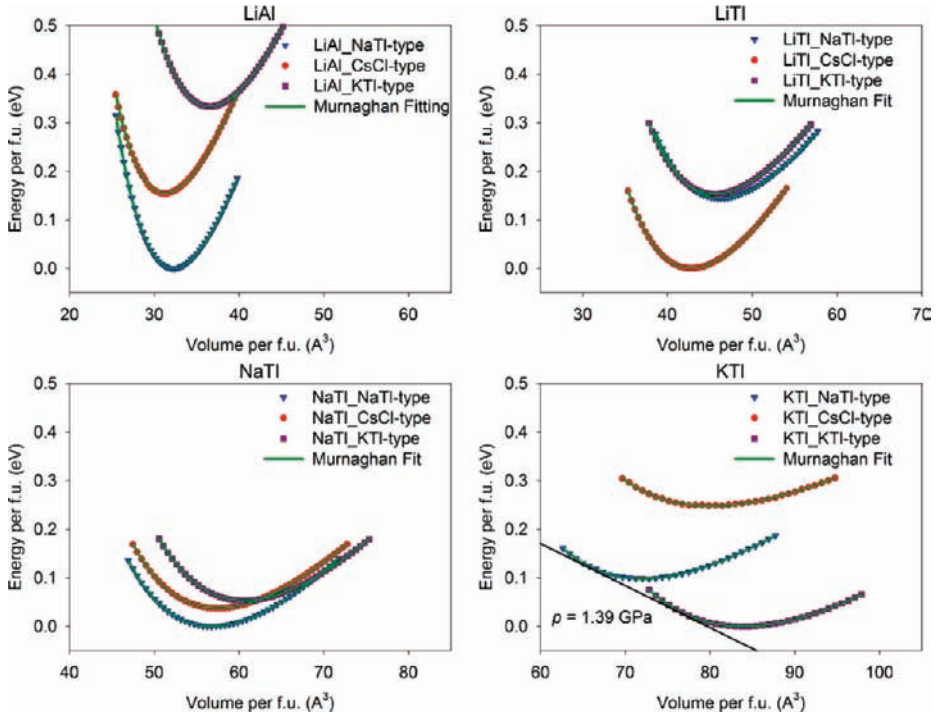

Figure 5. $E_{TOT}(V)$ curves of LiAl, LiTl, NaTl, and KTl in the NaTl-, CsCl-, and KTl-type structures.

values at the same volume, (1) Na has a smaller IDOS value than does Li and (2) Tl has higher IDOS in NaTl than in LiTl. This means that Na donates more valence electrons to Tl. It is in accordance with the electronegativity values of Li and Na. The absolute electronegativities are 3.01 eV for Li and 2.85 eV for Na.[64]

The optimum number of valence electrons for covalent bonding in a diamond structure is 4 per atom. Fewer valence electrons will weaken the bonds and destabilize the structure. For instance, when doping boron into silicon, according to the phase diagram,[65] the maximum amount of doping is 3.06% atom of boron at 1385 °C and much lower at room temperature. The same principle applies for the Tl diamond-type sublattice in the NaTl-type structure. To achieve 4 valence electrons per Tl, the alkali metal atoms must donate all valence electrons (1 per atom). In NaTl-type LiTl and NaTl, neither Li nor Na donates all valence electrons, but because Na donates more than Li, it affords stronger Tl−Tl bonding and stabilizes the Tl diamond sublattice better.

In conclusion, among LiAl, LiTl, and NaTl, LiTl gains the least stabilization from triel−triel covalent interactions in the NaTl-type structure. This is why covalency is overruled by metallicity and ionicity in LiTl and it defies the Zintl−Klemm rule, adopting the CsCl-type structure.

3. Volume Effects. In all discussions above, we have been comparing the CsCl- and the NaTl-type structures at equal volume per fu. This treatment successfully revealed the factors that are independent from volume, including relativistic effects and differences in charge transfer. However, it is unphysical; in reality, iso-compositional structures (polymorphs) do not have to have equal volumes per fu. For instance, at room temperature, the volume of diamond is 5.6730 Å^3/atom[66] and of graphite is 8.8214 Å^3/atom.[67] Therefore, the CsCl- and the NaTl-type structures may gain their maximum stability at different volumes as well, and the volume difference should also be considered.

To study such volume effects, we varied the volume and examined how the total energy responds in the CsCl- and the NaTl-types LiAl, LiTl, and NaTl (Figure 5). The calculated $E_{TOT}(V)$ curves were fitted with the Murnaghan equation of state,[37] from which we obtained the bulk moduli of these phases. The calculated bulk moduli of LiAl and NaTl in their observed double diamond structure are, respectively, 4.71×10^{11} and 1.75×10^{11} dyne/m^2, which are only slightly smaller than the experimental values, 5.07×10^{11} and 1.86×10^{11} dyne/m^2.[68] Moreover, we also obtained the equilibrium volumes (V_{eq}), that is, the volume at the minima of the curves (Table 6). These are the predicted volumes of the corresponding structures at zero pressure and 0 K. The energy terms and ICOHP were calculated for all structures at their V_{eq} and also tabulated in Table 6.

In general, VASP predicts volumes larger than the experimental values, especially for thallides. This can be attributed to the PBE-GGA[33] used in VASP, an approximation that has been found to overestimate lattice parameters.[69,70] Despite this defect, VASP does predict the right structure for each composition; the overall minima occur in the curves of the NaTl-type structure for LiAl and NaTl, and in the curve of the CsCl-type structure for LiTl.

The CsCl- and the NaTl-type structures have different V_{eq}. The difference ΔV_{eq} with respect to the CsCl-type is much larger in LiTl (+3.30 Å^3/fu) than in LiAl (+0.98 Å^3/fu) and NaTl (−0.67 Å^3/fu). This can be explained by examining the radius ratios between the alkali metal (r_A) and the triel atoms (r_{triel}). The two structures will have the same volume when $r_A/r_{triel} = 1$, while the greater this ratio deviates from 1, the larger is the volume difference. The covalent radii of Li, Na, Al, and Tl are, respectively, 1.28(7), 1.66(9), 1.21(4), and 1.45(7) Å.[71] LiAl has a smaller ΔV_{eq} than LiTl because r_{Li}/r_{Al} (1.06) is closer to 1 than is r_{Li}/r_{Tl} (0.88). r_{Na}/r_{Tl} (1.14) is slightly farther from 1 than is

dx.doi.org/10.1021/ic200643f |Inorg. Chem. 2011, 50, 7625–7636

Table 6. Equilibrium Volumes Obtained from Fitting $E(V)$ Curves and the Energy Terms and ICOHP Calculated at These Equilibrium Volumes[a]

	LiAl	LiTl	NaTl	KTl
V_{exp} (Å^3/fu)	31.84	40.64	51.61	78.32
$V_{eq,CsCl\text{-}type}$ (Å^3/fu)	31.28	42.81	57.49	80.07
$V_{eq,NaTl\text{-}type}$ (Å^3/fu)	32.26	46.21	56.82	72.00
$\Delta E_{ES,CsCl\text{-}type}$ (eV/fu)	0	0	0	0
$\Delta E_{ES,NaTl\text{-}type}$ (eV/fu)	2.0842	2.9681	0.8046	−5.5255
$\Delta E_{electronic,CsCl\text{-}type}$ (eV/fu)	0	0	0	0
$\Delta E_{electronic,NaTl\text{-}type}$ (eV/fu)	−2.2390	−2.9237	−0.8417	5.3759
$\Delta E_{TOT,eq,CsCl\text{-}type}$ (eV/fu)	0	0	0	0
$\Delta E_{TOT,eq,NaTl\text{-}type}$ (eV/fu)	−0.1548	0.1444	−0.0371	−0.1496
$ICOHP_{triel-triel,CsCl\text{-}type}$ (eV/fu)	−1.59	−0.84	−0.66	−0.69
$ICOHP_{triel-triel,NaTl\text{-}type}$ (eV/fu)	−3.36	−1.87	−1.62	−1.65
$\Delta E_{Madelung,CsCl\text{-}type}$ (eV/fu)	0	0	0	0
$\Delta E_{Madelung,NaTl\text{-}type}$ (eV/fu)	1.3984	1.3658	1.0480	0.7513

[a] The energy terms of the CsCl-type structures are taken as reference.

r_{Li}/r_{Tl}. The smaller and negative ΔV_{eq} of NaTl than LiTl can be attributed to the higher compressibility of the larger atoms, Na in NaTl than Tl in LiTl.

The large positive ΔV_{eq} will make the NaTl-type structure even more unfavorable by E_{ES}. Besides the difference in Madelung constant, E_{ES} is inversely proportional to R_a or $V^{1/3}$.[46,47] Table 6 shows that E_{ES} are higher in the NaTl-type structure for LiAl, LiTl, and NaTl. Also, LiTl has the most positive ΔV_{eq} among the three so it also has the most positive ΔE_{ES}. So the previous reports whose arguments are based on "size effects"[55−57] are right in this point: it is beneficial for the NaTl-type structure to have an r_A/r_{triel} close to 1, and the larger atom has good compressibility. However, the reason is not that the smaller atoms want to be in close contact, because LiTl adopts the CsCl-type structure where Li−Li distances are even larger ($r_{eq,Li-Li}$ = 3.498 Å) than in the NaTl-type structure ($r_{eq,Li-Li}$ = 3.108 Å).

$E_{electronic}$ are still always lower in the NaTl-type structure. Here, besides valence electron localization, volume also has an effect in $E_{electronic}$. When two structures are compared at different volumes, their average valence electron densities (n) are different. Both $V_{HEG-HEG}$ and T_{HEG} are functionals of n so they also contribute to $\Delta E_{electronic}$ (eq 4). Currently, we cannot precisely calculate these two terms, so we cannot quantitatively evaluate the effect of valence electron localization from $\Delta E_{electronic}$ yet. However, ICOHP values suggest that triel−triel covalent interactions still provide more stabilization in the NaTl-type structure; it always has lower ICOHP values. Also, ionicity still favors the CsCl-type structures; we calculated the ionic Madelung energy, $E_{Madelung}$, with the Ewald technique,[52] and it is always positive for the NaTl-type structures.

Therefore, comparisons at different V_{eq} achieve the same conclusion; covalency favors the NaTl-type structure and competes with metallicity, which favors the CsCl-type structure. Finally, ΔE_{TOT} shows that volume relaxation of the two structures does not change their relative stability; E_{TOT} is still lower for the NaTl-type structure in LiAl and NaTl and higher in LiTl.

4. The KTl-type Structure. The distorted Tl_6^{6-} octahedra in the KTl-type structure, as previously mentioned, resemble gaseous Si_6. Therefore, it can also be perceived as a structure stabilized by the covalent interactions between pseudo tetrel atoms. Rather than the O_h symmetry of a regular octahedron, the Tl_6^{6-} octahedron is "compressed" and exhibits C_{2h} symmetry.[24] This is a Jahn−Teller type distortion and can be seen by analyzing the MO diagrams (calculated with GAMESS[72,73]) of a single Tl_6^{6-} cluster as well as the band structure of KTl (Figure 6). The MO of single octahedrally symmetric Tl_6^{6-} cluster has an open shell electronic configuration; the triply degenerate HOMO, t_{1u}, is not fully occupied. By distorting into C_{2h} symmetry, the t_{1u} MO splits into three b_u orbitals and achieves a close shell configuration. This degeneracy lowering of HOMO manifests as a band gap opening at the Fermi level in the band structures. We can also see the consistency between the MO sketch of the LUMO in C_{2h} Tl_6^{6-} and the valence electron density map of the lowest unoccupied band in KTl (the insets in Figure 6). Besides such geometric distortion, Tl_6^{6-} octhedra can be further stabilized by relativistic spin−orbit coupling effects, as shown by Jansen[74] with Tl_8^{6-} in $Cs_{18}Tl_8O_6$. Our former report also showed that spin−orbit coupling broadens the band gap in KTl.[62] Therefore, the KTl-type structure satisfies the Zintl−Klemm concept well; it can be rationalized by considering merely the covalent interactions between "anions". The mystery here is how to understand the competition between this structure and the NaTl-type structure, which are both stabilized by covalency.

To study the stability of the KTl-type structure relative to the NaTl-type structure, we compared these two structures for two compositions, NaTl and KTl (Table 7), at two volumes, 51.61 and 78.32 Å^3/fu, the experimental volumes of NaTl and KTl.[16,24] The total energy values reveal that volume has a determining effect here. At 51.61 Å^3/fu, ΔE_{TOT} (=E_{TOT}(KTl-type) − E_{TOT}(NaTl-type)) is always positive, so the NaTl-type structure is energetically favored by both NaTl and KTl. Yet at 78.32 Å^3/fu, the KTl-type structure is favored for both compositions. ΔE_{ES} and $\Delta E_{Madelung}$ are always positive, so the NaTl-type structure is lower in E_{ES} and $E_{Madelung}$, meaning that the KTl-type structure is an even worse solution than the NaTl-type structure for metallicity and ionicity.

ΔICOHP has the same signs with ΔE_{TOT}, suggesting that at 51.61 Å^3/fu, the NaTl-type structure affords stronger Tl−Tl "bonding", while at 78.32 Å^3/fu, the KTl-type structure has stronger Tl−Tl orbital interactions. Such a volume effect on covalency can be attributed to Tl−Tl interatomic distances (Table 8). The symmetry of the NaTl-type requires equal alkali−alkali (r_{A-A}), alkali−Tl (r_{A-Tl}), and Tl−Tl (r_{Tl-Tl}) distances (if we only consider the nearest neighbors), whereas there is no such restriction in the KTl-type structure. As a result, the KTl-type structure can provide shorter Tl−Tl distances than the NaTl-type structure. At 78.32 Å^3/fu, most $r_{Tl-Tl,KTl\text{-}type}$ are much shorter than $r_{Tl-Tl,NaTl\text{-}type}$ by as much as 0.60 Å, so the KTl-type structure affords stronger Tl−Tl interactions. At 51.61 Å^3/fu, some $r_{Tl-Tl,KTl\text{-}type}$ are still shorter than $r_{Tl-Tl,NaTl\text{-}type}$ but to a smaller degree (0.07−0.25 Å), and more $r_{Tl-Tl,KTl\text{-}type}$ are longer than $r_{Tl-Tl,NaTl\text{-}type}$. Here, the KTl-type structure is no longer advantageous for covalency than the NaTl-type structure.

From Table 8, we can also see that, even at the same volume, KTl always has shorter Tl−Tl distances than NaTl. This is because K (covalent radius 2.03 Å[69]) is larger than Na (1.66 Å), so it "squeezes" Tl atoms closer to one another, which also enhances Tl−Tl covalent interactions.

dx.doi.org/10.1021/ic200643f |Inorg. Chem. 2011, 50, 7625–7636

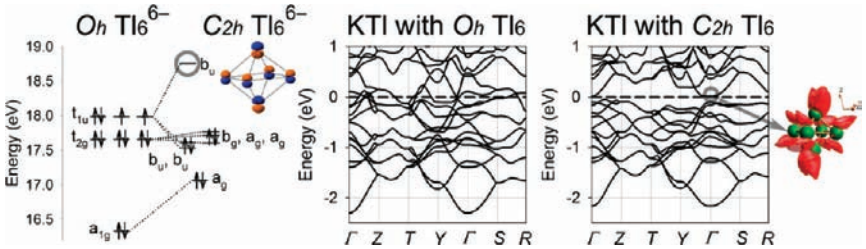

Figure 6. The frontier MO diagrams of O_h and C_{2h} Tl_6^{6-}, as compared to the band structures of KTl with O_h and C_{2h} Tl_6.

Table 7. Difference in Energy Terms, $\Delta E = E$(KTl-type) − E(NaTl-type), between the NaTl- and KTl-type Structures for NaTl and KTl Calculated at Two Fixed Volumes, Which Are the Experimental Volumes of NaTl and KTl

composition		51.61 Å^3/fu	78.32 Å^3/fu
NaTl	ΔE_{TOT} (eV/fu)	0.7675	−0.0681
	ΔE_{ES} (eV/fu)	9.4053	4.1630
	$\Delta E_{electronic}$ (eV/fu)	−8.6378	−4.2311
	$\Delta E_{Madelung}$ (eV/fu)	0.4991	0.9889
	ΔICOHP$_{Tl-Tl}$ (eV/fu)	0.24	−0.09
KTl	ΔE_{TOT} (eV/fu)	0.4476	−0.0863
	ΔE_{ES} (eV/fu)	3.4376	8.1848
	$\Delta E_{electronic}$ (eV/fu)	−2.9900	−8.2711
	$\Delta E_{Madelung}$ (eV/f.u.)	1.1426	1.5359
	ΔICOHP$_{Tl-Tl}$ (eV/fu)	0.38	−0.35

Therefore, the competition between these two covalency stabilized structures is determined by volume. At small volume, the diamond network can provide efficient Tl−Tl covalent interactions and is stabilized. At large volume, the diamond network cannot afford efficient covalent interactions as the Tl−Tl distances get too long. So, it is less stable with respect to the Tl_6^{6-} octahedron, which can still retain short Tl−Tl distances and, thus, efficient covalent interactions. KTl has a much larger volume than NaTl, so it adopts the Tl_6^{6-} octahedron as a structural motif rather than the double diamond structure. However, when compressed, KTl can transform into the NaTl-type structure, as shown by both experiment[26] and theory (Figure 5). Here, we predicted a phase transformation pressure at 1.39 GPa at 0K, over 6 times the experimentally determined value, 0.2 GPa, at room temperature.

5. Other Common "Metallic", "Ionic", and "Covalent" Structures. All of the discussions above have shown that Zintl phases such as alkali metal trielides are at the "frontier" where metallicity, ionicity, and covalency compete with one another. Therefore, it will be valuable and informative to construct them into structures that are commonly observed among metals, ionic crystals, and covalent crystals, and compare their energy terms and electronic structures. Table 9 compares the energy terms of the seven structure types calculated with VASP, the triel−triel distances in these structures, the ICOHP values calculated with LMTO, and the ionic Madelung energies calculated with the Ewald technique[52] assuming a +1 charge on each alkali metal atom and a −1 charge on each triel atom. These results are all calculated at equal volumes per fu for each composition. The Supporting Information also includes the DOS and COHP curves of these structures calculated with LMTO.

In the NaTl-, BaCu-, and KTl-type structures, the Al/Tl substructures are, respectively, diamond, graphite sheets, and distorted $(Al/Tl)_6$ octahedra. These are all structures adopted by tetrels, either in the solid or in the gaseous states, so they satisfy the Zintl−Klemm rule. The CsCl- and the NaCl-type structures cannot be rationalized with the Zintl−Klemm rule and are commonly observed in ionic crystals. Metals are known for adopting fcc and hcp structures. So the CuAu- (fcc) and AuCd-type (hcp) structures are expected to be favored by metallic systems. However, they also satisfy the octet rule and thus the Zintl−Klemm formalism; in these two structures, every triel atom is also "bonded" to four neighboring triel atoms (Figure 1). In the fcc-like, CuAu-type structure, triel atoms form planar sheets of squares, and in the hcp-like, AuCd-type structure, they form puckered sheets of squares.

By comparing the triel−triel distances in these equivolume structures (Table 9), we see that for each composition, the NaTl-, KTl-, and BaCu-type structures have the smallest $r_{triel-triel}$ (except in LiTl because Li is too small, and thus Tl atoms are set farther apart to fill the space). Their DOS and COHP curves (Supporting Information) reveal features resembling covalent crystals; the Fermi levels are located at the crossover in COHP curves between filled bonding and empty antibonding states, that is, bond optimization, and, in DOS curves, at state-deficient regions, that is , pseudogaps. The smallest $r_{triel-triel}$ and "bond optimization" for these three structure types also result in the most negative, that is, lowest, ICOHP values (again, with the KTl-type LiTl as an exception). Therefore, we conclude that these three structure types gain the largest stabilization through triel−triel covalent interactions.

On the other hand, the NaCl- and the CsCl-type structures have the largest $r_{triel-triel}$ values. Consequently, they have the weakest triel−triel interactions, and the ICOHP values are the highest among all. So, these two structure types experience the least stabilization through triel−triel covalent interactions. The CuAu- and the AuCd-type structures have intermediate $r_{triel-triel}$ values and optimized triel−triel COHP curves (Supporting Information), in accordance with fitting into the Zintl−Klemm formalism. Their ICOHP values are also intermediate, higher than the NaTl-, KTl-, and BaCu-types, and lower than the NaCl- and CsCl-type structures.

By comparing the energy terms in Table 9, above all, the ΔE_{TOT} (the E_{TOT} values of the CsCl-type structures are taken as reference) values predict the correct structures; for all compositions, the lowest ΔE_{TOT} occurs at the experimentally observed structure types. $\Delta E_{electronic}$, quantifying solely the effects of valence electron localization including covalent bonding, shows the same pattern as the ICOHP values, the lowest energies for the NaTl-, KTl-, and BaCu-type and the highest energies for the NaCl- and CsCl-type. ΔE_{ES}, reflecting metallicity, and $\Delta E_{Madelung}$, reflecting

dx.doi.org/10.1021/ic200643f |Inorg. Chem. 2011, 50, 7625–7636

Table 8. Comparisons in the Tl−Tl Interatomic Distances between the KTl- and the NaTl-type Sructures for NaTl and KTl at Two Fixed Volumes, Which Are the Experimental Volumes of NaTl and KTl[a]

volume:			51.61 Å^3/fu						78.32 Å^3/fu			
$r_{Tl-Tl,NaTl\text{-}type}$:			3.224 Å						3.705 Å			
composition:		NaTl			KTl			NaTl			KTl	
$r_{Tl-Tl,KTl\text{-}type}$	Tl1 −	Tl1	3.292 Å	Tl1 −	Tl1	3.319 Å	Tl1 −	Tl1	3.820 Å	Tl1 −	Tl1	**3.482** Å
			3.575 Å			3.324 Å			3.839 Å			**3.610** Å
			3.605 Å			3.527 Å			4.059 Å		Tl2	**3.107**Å
		Tl2	**3.150** Å		Tl2	**2.969** Å		Tl2	**3.333** Å			**3.130** Å
			3.152 Å			**3.013** Å			**3.358** Å	Tl2 −	Tl2	3.708 Å
				Tl2 −	Tl2	3.508 Å	Tl2 −	Tl2	**3.703** Å			

[a] The bold numbers are those distances shorter than $r_{Tl-Tl,NaTl\text{-}type}$.

Table 9. Energy Terms of the Seven Structure Types for LiAl, LiTl, NaTl, and KTl[a]

		NaTl-type	KTl-type	BaCu-type	CsCl-type	NaCl-type	CuAu-type (fcc)	AuCd-type (*h*cp)
LiAl 31.84 Å^3/fu	ΔE_{TOT} (eV/fu)	**−0.1553**	0.2651	0.1188	0	1.0487	−0.0235	−0.0734
	ΔE_{ES} (eV/fu)	1.3064	5.2514	3.5190	0	0.4137	1.1189	1.2783
	$\Delta E_{electronic}$ (eV/fu)	−1.4617	−4.9863	−3.4002	0	0.6350	−1.1424	−1.3517
	r_{Al-Al} (Å)	2.745	2.652 − 2.790	2.489	3.169	3.557	2.824	2.824
	$ICOHP_{Al-Al}$ (eV/fu)	−3.35	−3.12	−2.50	−1.56	−0.53	−2.51	−2.60
	$\Delta E_{Madelung}$ (eV/fu)	1.3076	2.1882	1.3555	0	−0.7562	1.1165	1.2723
LiTl 40.64 Å^3/fu	ΔE_{TOT} (eV/fu)	0.1985	0.1944	0.4475	**0**	0.4370	0.1285	0.0921
	ΔE_{ES} (eV/fu)	1.2054	0.5543	2.6584	0	0.3831	1.0329	1.1785
	$\Delta E_{electronic}$ (eV/fu)	−1.0069	−0.3599	−2.2108	0	0.0539	−0.9044	−1.0864
	r_{Tl-Tl} (Å)	2.977	3.271 − 3.624	2.746	3.438	3.859	3.063	3.063
	$ICOHP_{Tl-Tl}$ (eV/fu)	−2.03	−1.51	−2.07	−0.88	−0.42	−1.58	−1.66
	$\Delta E_{Madelung}$ (eV/fu)	1.2054	1.2554	1.1663	0	−0.6971	1.0293	1.1728
NaTl 51.61 Å^3/fu	ΔE_{TOT} (eV/fu)	**−0.0446**	0.0758	0.1590	0	0.4161	0.0027	−0.0286
	ΔE_{ES} (eV/fu)	1.1131	2.8263	3.3329	0	0.3534	0.9534	1.0886
	$\Delta E_{electronic}$ (eV/fu)	−1.1577	−2.7505	−3.1739	0	0.0627	−0.9506	−1.1172
	r_{Tl-Tl} (Å)	3.224	3.150 − 3.732	2.886	3.723	4.179	3.317	3.317
	$ICOHP_{Tl-Tl}$ (eV/fu)	−1.80	−1.56	−1.63	−0.74	−0.31	−1.31	−1.37
	$\Delta E_{Madelung}$ (eV/fu)	1.1131	1.6122	1.3041	0	−0.6437	0.9504	1.0829
KTl[b] 78.32 Å^3/fu	ΔE_{TOT} (eV/fu)	−0.1338	**−0.2328**	−0.1587	0	0.3637	0.0227	−0.0119
	ΔE_{ES} (eV/fu)	0.9686	8.0375	5.5078	0	0.3082	0.8307	0.9481
	$\Delta E_{electronic}$ (eV/fu)	−1.1024	−8.2703	−5.6665	0	0.0555	−0.8080	−0.9600
	r_{Tl-Tl} (Å)	3.705	3.107 − 3.708	3.133	4.278	4.802	3.812	3.812
	$ICOHP_{Tl-Tl}$ (eV/fu)	−1.43	−1.78	−1.98	−0.69	−0.16	−1.04	−1.06
	$\Delta E_{Madelung}$ (eV/fu)	0.9686	2.5046	1.4665	0	−0.5601	0.8272	0.9425

[a] For each composition, all structures have the same volume per fu. [b] For KTl in its own structure, the data are from the structure optimized with VASP instead of experimental structure from ref 24. The comparison between the optimized and experimental structures can be found in the Supporting Information.

ionicity, both reveal the exact opposite trend, the highest in the NaTl-, KTl-, and BaCu-types, and the lowest in the NaCl- and CsCl-types. These comparisons reveal that metallicity, ionicity, and covalency have opposite structural preferences. Metallicity and ionicity prefer high symmetry and more isotropic structures, while covalency favors less isotropic structures that afford shorter and optimized orbital interactions between electronegative atoms. Therefore, any rationalization of the structures of Zintl and polar intermetallic phases, where metallicity, ionicity, and covalency are competing, should not be based solely on covalency, as the Zintl−Klemm concept suggests, but on the competition between all three competitors, as we have demonstrated above with our analysis of alkali metal trielides.

CONCLUSIONS

By investigating the alkali metal trielides, LiAl, LiTl, NaTl, and KTl, to understand the structures of Zintl phases, it is insufficient to consider just the effects of covalent interactions between electronegative atoms as in the Zintl−Klemm formalism. Instead, they should be rationalized by examining the competition among metallic, ionic, and covalent effects. Any factors that can enhance or weaken metallic, ionic, and covalent interactions can affect their competition and cause structural variation among isoelectronic and "isocompositional" cases. Several influential factors were identified in our investigation: relativistic effects, electronegativity differences, and atomic size ratios between

dx.doi.org/10.1021/ic200643f |*Inorg. Chem.* 2011, 50, 7625–7636

constituent elements. Relativistic effects contract the 6s orbitals of Tl atoms and hinder them from participating in covalent interactions, rendering Tl−Tl covalent interactions relatively weaker than Al−Al ones in their structures. Electronegativity differences determine the degree of valence electron transfer from the electropositive atoms to the electronegative atoms. Greater transfer in alkali metal trielides can strengthen the covalent interactions between the electronegative atoms. The atomic size ratio is one of the reasons that LiTl forms the CsCl-type structure and also explains why KTl contains Tl_6^{6-} octahedra rather than the double diamond structure at ambient pressure. These findings deepen our understanding about the complete structures of Zintl phases.

■ ASSOCIATED CONTENT

Supporting Information. Optimized KTl- and BaCu-type structures, the DOS and COHP curves of LiAl, LiTl, NaTl, and KTl in the seven structure types, the valence electron density maps of CsCl-type LiAl, LiTl, and NaTl, the sp projections of the wave functions at Γ- and *L*-points, and the electron density maps of the bands at Γ- and *L*-points. This material is available free of charge via the Internet at http://pubs.acs.org.

■ AUTHOR INFORMATION

Corresponding Author

*Phone: 515-294-6063. Fax: 515-294-9623. E-mail: gmiller@iastate.edu.

■ ACKNOWLEDGMENT

This work was supported by NSF DMR 06-05949 and 10-05765. The computations were done on the CRUNCH system supported by Iowa State University Computation Advisory Committee project 202-17-10-08-0005.

■ REFERENCES

(1) Anderson, W. P.; Burdett, J. K.; Czech, P. T. *J. Am. Chem. Soc.* **1994**, *116*, 8808.
(2) Zintl, E.; Dullenkopf, W. *Z. Phys. Chem.* **1932**, *B16*, 183.
(3) Zintl, E.; Brauer, G. *Z. Phys. Chem.* **1933**, *B20*, 245.
(4) Zintl, E. *Angew. Chem.* **1939**, *52*, 1.
(5) Schäfer, H.; Eisenmann, B.; Müller, W. *Angew. Chem., Int. Ed. Engl.* **1973**, *12*, 694.
(6) Schäfer, H.; Eisenmann, B. *Rev. Inorg. Chem.* **1981**, *3*, 29.
(7) Schäfer, H. *Annu. Rev. Mater. Sci.* **1985**, *15*, 1.
(8) Nesper, R. *Prog. Solid State Chem.* **1990**, *20*, 1.
(9) *Chemistry, Structure, and Bonding of Zintl Phases and Ions*; Kauzlarich, S. M., Ed.; VCH: Weinheim, Germany, 1996.
(10) Kanatzidis, M. G. *Recent Trends in Thermoelectric Materials Research I Series: Semiconductors and Semimetals*; Academic: San Diego, CA, 2001; Vol. 69, p 51.
(11) Gascoin, F.; Ottensmann, S.; Stark, D.; Haïle, S. M.; Snyder, G. J. *Adv. Funct. Mater.* **2005**, *15*, 1860.
(12) Shawna, R. B.; Kauzlarich, S. M.; Gascoin, F.; Snyder, G. J. *Chem. Mater.* **2006**, *18*, 1873.
(13) Condron, C. L.; Kauzlarich, S. M. *Inorg. Chem.* **2007**, *46*, 2556.
(14) Kauzlarich, S. M.; Brown, S. R.; Snyder, G. J. *Dalton Trans.* **2007**, 2099.
(15) Snyder, G. J.; Toberer, E. S. *Nat. Mater.* **2008**, *7*, 105.
(16) Zintl, E.; Woltersdorf, G. *Z. Elektrochem.* **1935**, *41*, 876.
(17) Seifert-Lorenz, K.; Hafner, J. *Phys. Rev. B* **1999**, *59*, 829.
(18) Genser, O.; Hafner, J. *J. Phys.: Condens. Matter* **2001**, *13*, 959.
(19) Seifert-Lorenz, K.; Hafner, J. *Phys. Rev. B* **2002**, *66*, 094105–1.
(20) Baden, W.; Schmidt, P. C.; Weiss, A. *Phys. Status Solidi A* **1979**, *51*, 183.
(21) Ehrenberg, H.; Pauly, H.; Knapp, M.; Gröbner, J.; Mirkovic, D. *J. Solid State Chem.* **2004**, *177*, 227.
(22) Jang, G. E.; Curelaru, I. M.; Hentschel, M. P. *J. Cryst. Growth* **1994**, *141*, 399.
(23) Pauly, H.; Weiss, A.; Witte, H. *Z. Metallkd.* **1968**, *59*, 554.
(24) Dong, Z.; Corbett, J. D. *J. Am. Chem. Soc.* **1993**, *115*, 11299.
(25) Honea, E. C.; Ogura, A.; Murray, C. A.; Raghavachari, K.; Sprenger, W. O.; Jarrold, M. F.; Brown, W. L. *Nature* **1993**, *366*, 42.
(26) Evers, J.; Oehlinger, G. *Inorg. Chem.* **2000**, *39*, 628.
(27) Grube, V. G.; Schmidt, A. *Z. Elektrochem.* **1936**, *42*, 201.
(28) Wang, F.; Miller, G. J. *Eur. J. Inorg. Chem.* **2011**, in press.
(29) (a) Kresse, G.; Hafner, J. *Phys. Rev. B* **1993**, *47*, 558. (b) Kresse, G.; Hafner, J. *Phys. Rev. B* **1994**, *49*, 14251.
(30) Kresse, G.; Furthmüller, J. *Comput. Mater. Sci.* **1996**, *6*, 15.
(31) Kresse, G.; Furthmüller, J. *Phys. Rev. B* **1996**, *54*, 11169.
(32) Kresse, G.; Joubert, D. *Phys. Rev.* **1999**, *59*, 1758.
(33) Perdew, J. P.; Burke, K.; Ernzerhof, M. *Phys. Rev. Lett.* **1996**, *77*, 3865.
(34) Monkhorst, H. J.; Pack, J. D. *Phys. Rev. B* **1976**, *13*, 5188.
(35) Eck, B. *wxDragon*, version 1.4.2; RWTH Aachen University: Aachen, Germany, 2008.
(36) Press, W. H.; Flannery, B. P.; Teukolsky, S. A.; Vetterling, W. T. *Numerical Recipes*; Cambridge University Press: New York, 1986.
(37) Murnaghan, F. D. *Proc. Natl. Acad. Sci. U.S.A.* **1944**, *30*, 244.
(38) Jepsen, O.; Andersen, O. K. *TB-LMTO*, version 47; Max-Planck-Institut für Festkörperforschung: Stuttgart, Germany, 2000.
(39) Dronskowski, R.; Blöchl, P. *J. Phys. Chem.* **1993**, *97*, 8617.
(40) Grechnev, A.; Ahuja, R.; Eriksson, O. *J. Phys.: Condens. Matter* **2003**, *15*, 7751.
(41) Bester, G.; Fähnle, M. *J. Phys.: Condens. Matter* **2001**, *13*, 11541.
(42) Bester, G.; Fähnle, M. *Phys. Rev. B* **2005**, *B72*, 094102.
(43) von Barth, U.; Hedin, L. *J. Phys. C: Solid State Phys.* **1972**, *5*, 1629.
(44) Koelling, D.; Harmon, B. N. *J. Phys. C* **1977**, *10*, 3107.
(45) Skriver, H. L. In *The LMTO Method: Muffin-Tin Orbitals and Electronic Structure*; Cardona, M., Fulde, P., Queisser, H.-J., Eds.; Spring Series in Solid-State Sciences 41; Springer-Verlag: New York, 1984; p 82.
(46) Hafner, J. *From Hamiltonians to Phase Diagrams*; Springer-Verlag: New York, 1987.
(47) Fuchs, K. *J. Phys.: Condens. Matter* **1935**, *6*, 8245.
(48) Ashcroft, N. W.; Mermin, N. D. *Solid State Physics*; Brooks/Cole: U.S., 1976; p 38.
(49) Kohn, W.; Sham, L. J. *Phys. Rev.* **1965**, *140*, A1133.
(50) Barett, C. S. *Acta Crystallogr.* **1956**, *9*, 671.
(51) Kuestner, H.; Remy, H. *Phys. Z.* **1923**, *24*, 25.
(52) Ewald, P. P. *Ann. Phys. Leipzig* **1921**, *64*, 253.
(53) Miller, G. J. *Eur. J. Inorg. Chem.* **1998**, 523.
(54) Inglesfield, J. E. *J. Phys. C: Solid State Phys.* **1971**, *4*, 1003–1012.
(55) Pearson, W. B. *The Crystal Chemistry and Physics of Metals and Alloys*; Wiley-Interscience: New York, 1972; p 576.
(56) McNeil, M. B.; Pearson, W. B.; Bennett, L. H.; Watson, R. E. *J. Phys. C: Solid State Phys.* **1973**, *6*, 1.
(57) Schmidt, P. C. *Phys. Rev. B.* **1985**, *31*, 5015.
(58) Christensen, N. E. *Phys. Rev. B* **1985**, *32*, 207.
(59) Pawlowska, Z.; Christensen, N. E.; Satpathy, S.; Jepsen, O. *Phys. Rev. B* **1986**, *34*, 7080.
(60) Bilbao Crystallographic Server. http://www.cryst.ehu.es/ (accessed June 2010).
(61) Pitzer, K. S. *Acc. Chem. Res.* **1979**, *12*, 271.
(62) Miller, G. J.; Schmidt, M. W.; Wang, F.; You, T.-S. *Structure & Bonding*; Springer: online, 2011; DOI: 10.1007/430_2010_24.
(63) Dronskowski, R. *Computational Chemistry of Solid State Materials*; Wiley-VCH: Weinheim, Germany, 2005.
(64) Pearson, R. G. *Inorg. Chem.* **1988**, *27*, 734.
(65) *ASM Handbook, Alloy Phase Diagrams*; ASM International: U.S., 1992; Vol. 3.

(66) Hom, T.; Kiszenik, W.; Post, B. *J. Appl. Crystallogr.* **1975**, *8*, 457.
(67) Trucano, P.; Chen, R. *Nature* **1975**, *258*, 136.
(68) Kuriyama, K.; Saito, S.; Iwamura, K. *J. Phys. Chem. Solids* **1979**, *40*, 457.
(69) Haas, P.; Tran, F.; Blaha, P.; Schwarz, K.; Laskowski, R. *Phys. Rev. B* **2009**, *80*, 195109.
(70) Stoffel, R. P.; Wessel, C.; Lumey, M.-W.; Dronskowski, R. *Angew. Chem., Int. Ed.* **2010**, *49*, 2.
(71) Cordero, B.; Gómez, V.; Platero-Prats, A. E.; Revés, M.; Echeverría, J.; Cremades, E.; Barragán, F.; Alvarez, S. *Dalton Trans.* **2008**, 2832.
(72) Schmidt, M. W.; Baldridge, K. K.; Boatz, J. A.; Elbert, S. T.; Gordon, M. S.; Jensen, J. H.; Koseki, S.; Matsunaga, N.; Nguyen, K. A.; Su, S.; Windus, T. L.; Dupuis, M.; Montgomery, J. A. *J. Comput. Chem.* **1993**, *14*, 1347.
(73) Gordon, M. S.; Schmidt, M. W. Advances in electronic structure theory: GAMESS a decade later. In *Theory and Applications of Computational Chemistry: The First Forty Years*; Dykstra, C. E., Frenking, G., Kim, K. S., Scuseria, G. E., Eds.; Elsevier: Amsterdam, 2005; p 1167.
(74) Wedig, U.; Saltykov, V.; Nuss, J.; Jansen, M. *J. Am. Chem. Soc.* **2010**, *132*, 12458.